SSCL-Preprint-134

SSCL-Preprint-134

Superconducting Super Collider Laboratory

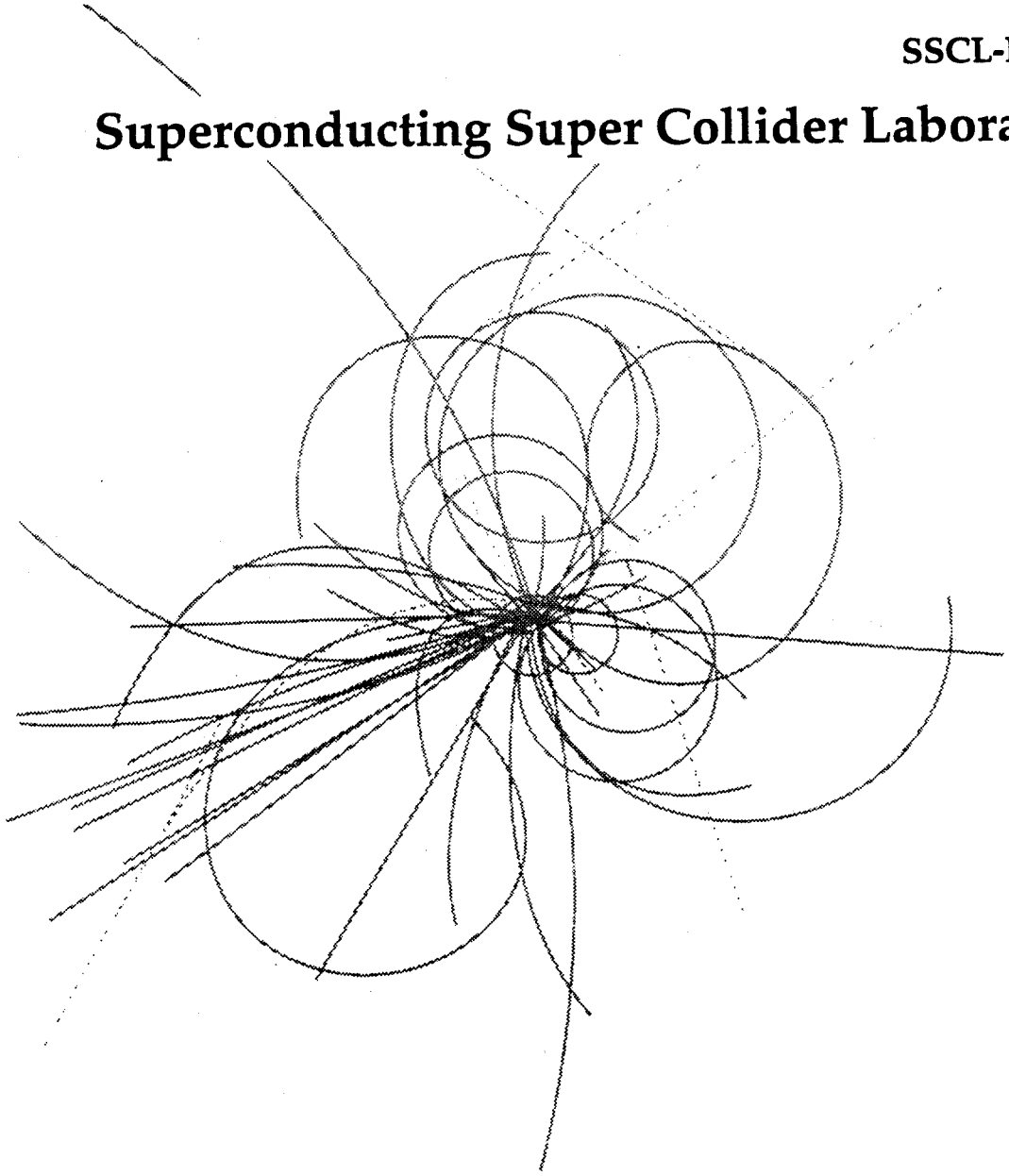

Influence of Cable Eddy Currents on Magnetic Field Harmonics

T. Ogitsu, Y. Zhao, A. Akhmetov, and A. Devred

July 1992

SSCL-Preprint-134

Influence of Cable Eddy Currents on Magnetic Field Harmonics

T. Ogitsu, Y. Zhao, A. Akhmetov, and A. Devred

Superconducting Super Collider Laboratory†
2550 Beckleymeade Ave.
Dallas, TX 75237

July 1992

†Operated by the Universities Research Association, Inc., for the U.S. Department of Energy under Contract No. DE-AC35-89ER40486.

Presented at the ICFA workshop on AC superconductivity, June 23-25, 1992, KEK, Tsukuba, Japan.

Influence of Cable Eddy Currents on Magnetic Field Harmonics

T. Ogitsu – SSC Laboratory,* Dallas, Texas, USA,
and KEK, National Laboratory for High Energy Physics, Tsukuba, Ibaraki, Japan

Y. Zhao, A. Akhmetov, and A. Devred – SSC Laboratory.

ABSTRACT

Several SSC 5-cm-aperture, 15-m-long dipole magnet prototypes exhibit anomalous behavior of their magnetic field harmonics during current ramps at 4 A/s. The anomalies cease when the ramp is stopped and the current is held constant. The magnets also exhibit a dramatic degradation of their quench current as a function of ramp rate, as well as large AC-losses. After reviewing the AC-performance of the anomalous magnets, we develop a model of cable eddy currents, which can simulate the observed field behavior and the measured AC-losses, and which is consistent with the quench start localization of the high ramp-rate quenches.

INTRODUCTION

A key issue in the operation of superconducting magnets for particle accelerator is the existence of current-dependent field distortions.

A well known cause for current-dependent field distortions is persistent magnetization currents in the superconductor. Persistent magnetization currents can be described using Bean's critical state model,[1] and their effects on the magnetic field can be computed using a software originally developed at Deutsches Elektronen-Synchrotron Laboratory (DESY). The DESY software relies on the critical state model, but the persistent-magnetization current shells are assumed to be elliptical.[2] This software was very successful in predicting the behavior of the superconducting magnets for HERA.[3] It is also quite successful in predicting the behavior of most of the SSC superconducting dipole and quadrupole magnet prototypes.[4] This repeated agreement gives good confidence that the effects of the persistent magnetization currents can be reliably predicted.

It was recently reported, however, that four 15-m-long, 5-cm-aperture SSC dipole magnet prototypes (magnets DCA312, DCA313, DCA314, and DCA315) exhibited field variations during current ramping which significantly differed from other SSC dipole magnet prototypes, and which could not be explained by the persistent magnetization current model.[5] It was also observed that this anomalous behavior only appeared while ramping the current, and that it ceased when the ramp was stopped and the current held constant. Aside of this anomalous field behavior, these four magnets exhibited a dramatic degradation of their quench current as a function of ramp rate.[6] At large ramp rates, they also appeared to dissipate two to four times more AC-losses than magnets which did not exhibit anomalies in their field harmonics.[7] The strong ramp-rate sensitivity, and the large AC-losses were attributed to unexpectedly large cable eddy currents.[6,7] It is reasonable to think that these eddy currents are also the cause of the anomalous field behavior.

In this paper, we shall first review the experimental facts regarding the magnetic measurements and the quench performance of the four anomalous magnets. We shall then briefly describe a model that is being developed in order to simulate the effects of eddy currents on the magnetic field, and we shall show how this model can account for the observed anomalies.

TESTS RESULTS

Magnetic Field Harmonics

In the long, almost straight, section of the magnet, the field can be considered as two-dimensional, and is conveniently represented by a multipole expansion

$$B_y + iB_x = 10^{-4} B_0 \sum_{n=0}^{+\infty} (b_n + ia_n) \left(\frac{x+iy}{r_0}\right)^n \quad , \qquad (1)$$

where B_x and B_y are the x- and y-components of the field, B_0 is the dipole field strength, b_n and a_n are the normal and skew 2(n+1)-pole coefficients, and r_0 is the reference radius. (For the SSC magnets, r_0 = 1 cm.) The x-y coordinate system is defined perpendicularly to the beam line, with its origin at the beam center, and so that the y-axis is parallel to the normal dipole field. The symmetries of a dipole magnet are such that only even normal multipole coefficients, also called *allowed* multipole coefficients, are expected to be non-zero. In real magnets, manufacturing errors result in violations of the dipole symmetries which lead to non-zero *un-allowed* multipole coefficients. It can be shown, however, that, in first approximation, the persistent magnetization currents only affect the allowed multipole coefficients.[2]

'On the Fly' Measurements

The field harmonics are measured using a measuring system developed by Brookhaven National Laboratory.[8] This system, called the *mole*, consists of a tangential coil and two dipole bucking coils, which are 0.6 m in length, and rotate with a 3.2-s period. Eventual errors resulting from misalignment of the measuring system with respect to the magnet axis are corrected by re-computing the multipole coefficients so that either (a_7,b_7) or (a_9,b_9) are forced to be zero.

*Operated by the Universities Research Association, Inc., for the U.S. Department of Energy under Contract No. DE-AC35-89ER40486.

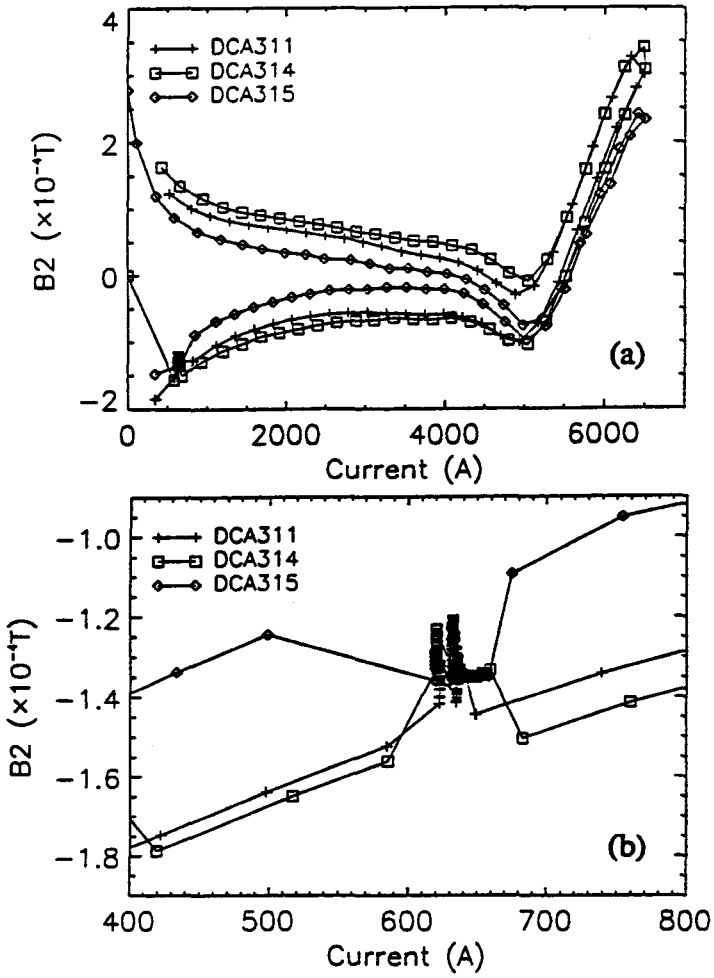

Fig. 1. Summary of B_1 as a function of current for two anomalous magnets (magnets DCA315 and DCA314) and a normally-behaved one (magnet DCA311): a) for the whole current range, and b) around the injection current.

The measurements are taken following a generic test sequence which includes both current-dependence and time-dependence measurements, and which is representative of a SSC operating cycle. The sequence starts with a *cleansing quench* to erase all previous persistent magnetization currents. The magnet is then *pre-cycled* to a current of 6500 A for a duration of 5 min, simulating a colliding beam cycle. It is then ramped down to 115 A for 2 min, ramped up to 620 A for 10 min (*pre-injection porch*), and ramped up again to 635 A for 1 hour (*injection porch*). At the end of the injection porch, the current is ramped up again to 6500 A, and then ramped down to 120 A, to simulate the next colliding beam cycle. The current ramp rate is 4 A/s, except for the ramp from 620 to 635 A, which is performed at 1 A/s. What we refer to as *time-dependence* measurements are the measurements taken while sitting at 620 and 635 A. The *current-dependence* measurements include all the measurements taken from the 120-A dwell following the pre-cycle until the end of the test sequence.

Figures 1 and 2 display typical measurement results. The multipole coefficients reported in these figures have been re-scaled using

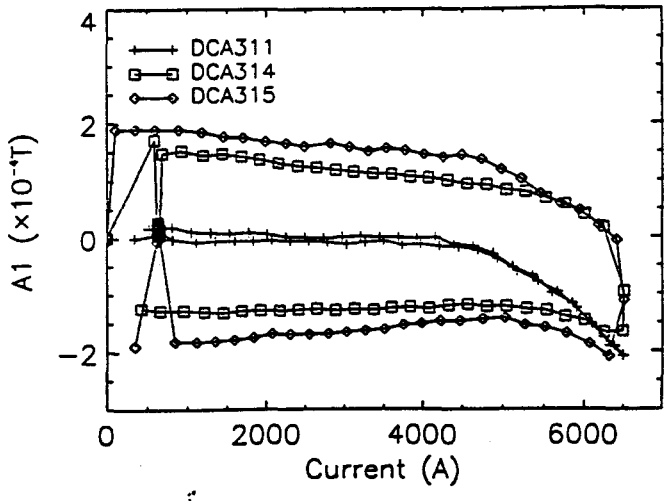

Fig. 2. Summary of A_1 as a function of current for two anomalous magnets (magnets DCA315 and DCA314) and a normally-behaved one (magnet DCA311).

$$B_n = B_0 [b_n - (b_{nu} + b_{nd})/2] \quad , \tag{2a}$$

and

$$A_n = B_0 [a_n - (a_{nu} + a_{nd})/2] \quad , \tag{2b}$$

where b_{nu} and a_{nu} designate the average values of b_n and a_n during the up-ramp from 2 kA to 3 kA, and b_{nd} and a_{nd} designate the average values of b_n and a_n during the down-ramp from 3 kA to 2 kA. (Note that, in the 2-to-3 kA range, the up- and down-ramp variations of the multipole coefficients are usually symmetrical.)

Figure 1.a shows a summary plot of B_2 as a function of current for two anomalous magnets (magnets DCA315 and DCA314) and a normally-behaved one (magnet DCA311). For the three traces, the bottom half of the plot corresponds to the current up-ramp. As expected from the effects of the persistent magnetization currents, all the traces, including that of the normal magnet, exhibit a large hysteresis. The width of this hysteresis, however, varies slightly magnet-to-magnet. Figure 1.b shows a blow-up of the previous plots for currents around the injection current. The data plotted in figure 1.b also include the time-dependence measurements taken while seating on the pre-injection and injection porches. It clearly appears that, when the ramp is stopped and the current is held constant, the traces of the two anomalous magnets converge towards that of magnet DCA311. (Note that for currents above 5 kA, the three traces of figure 1.a show a clear rise, attributed to iron yoke saturation effects.[9])

Figure 2 shows a similar summary plot for A_1 as a function of current. Although we are not expecting any sizable effects from the persistent magnetization currents, magnets DCA314 and DCA315 both exhibit a very large hysteresis. Furthermore, these two hystereses appear to be described in opposite direction: for magnet DCA314, the current up-ramp corresponds to the upper branch, while for magnet DCA315, it corresponds to the lower branch. In both cases, however, it can

clearly be seen that, upon reaching the pre-injection porch, the traces leap from their anomalous positions to a near-zero value, similar to that of magnet DCA311. (For currents above 4 to 5 kA, the three traces show a tendency to dip, attributed to flux leakage asymmetry between magnet cold mass and cryostat.[9])

In comparing figures 1.a and 2, it is interesting to note that, in the case of B_2, the width of the hysteresis decreases as a function of current, while, in the case of A_1, it remains roughly constant.

Behavior similar to that depicted in figures 1 and 2 can be seen in all the multipole coefficients up to the decapole. Magnets DCA312 and DCA314, for instance, exhibit an anomalous B_4 hysteresis, which is of a larger amplitude and of opposite sign to that predicted by the persistent magnetization current model, and to that exhibited by magnet DCA311. Similar to the lower order multipoles, however, the anomaly ceases upon reaching the pre-injection porch, where B_4 leaps to a value very close to the predicted one.

Ramp rate Sensitivity of the Quench Current and AC-Loss Measurements

As we already mentioned, magnets DCA312 through DCA315 exhibit a dramatic degradation of their quench current as a function of ramp rate.[6,7] These four magnets, which use cables from the same vendor, behave quite similarly: the quench current remains roughly constant for ramp rates up to 25 A/s, above which it starts to drop sharply. The most extreme case is magnet DCA312, which, at 200 A/s, quenches at about 2 kA, corresponding to 30% of the initial quench current. In comparison, the behavior of magnet DCA311, which uses cables from another vendor, is quite different: the quench current starts by dropping significantly at low ramp rates, from about 7.2 kA at 1 A/s to about 6.9 kA at 25 A/s. For larger ramp rates, however, the degradation is much milder, and, at 250 A/s, the quench current is still of the order of 5.5 kA, corresponding to 75% of the initial quench current. In all cases, the quenches at high ramp rates originate in a turn relatively close to the midplane of the inner coil. Tests were also carried out on some of the prototypes to determine their ramp-rate sensitivity on a down-ramp from 6500 A. No quenches, however, were observed for ramp rates up to 200 A/s.

AC-loss measurements were performed on three of the anomalous magnets (magnets DCA312, DCA314, and DCA315), as well as on magnet DCA311.[7] The measurements were made electrically, using a simple sawtooth ramp between 500 A and 5000 A, with ramp rates varying from 30 to 150 A/s. The losses appear to increase quasi-linearly as a function of ramp rate, and Table 1 summarizes the coefficients of a first order fitting of the experimental data.[7] As can be seen in Table 1, the AC-loss slopes of magnets DCA312, DCA314, and DCA315 are two to four times larger than that of magnet DCA311.

Table. 1. AC-Loss Measurement Summary[7] and Estimated Crossover Resistance.

Magnet	Intercept (J)	Slope (J/A/s)	X-over Res. (μΩ)
DCA311	530±130	16.2±1.3	12
DCA312	1160±220	57.3±3.6	3
DCA314	840±120	35.1±1.3	6
DCA315	780±150	50.9±2.2	4

EDDY CURRENTS DUE TO INTERSTRAND COUPLING

The SSC magnet coils are wound with Rutherford-type conductors.[10] These conductors consist of 30 or 36 strands, twisted together, and shaped into a flat, two-layer, slightly keystoned cable. The cable mid-thickness is smaller than twice the strand diameter, and the contact surfaces at the crossovers between the strands of the two layers are relatively large. Also, during magnet assembly, the coils are pre-compressed azimuthally. Large pressures are thus applied perpendicularly to the cables, which keep the strands firmly in contact. The large contact surfaces and high pressures eventually result in low contact resistances at the strand crossovers, which couple the cable strands. Loops are thus formed where significant eddy currents can be generated when subjected to a varying field. Assuming the eddy currents flowing from one strand to the other always pass through the crossover resistances, the cable can be represented by a simple model circuit.[11] The cable eddy currents can be computed by combining this model circuit with a two dimensional field calculation. The details of this computation will be described elsewhere.[12] The next step is to determine the effects of these eddy currents on the magnetic field.

The magnetic field has mainly three components: 1) a component, B_t, resulting from the transport current, I, circulating in the coil, 2) a component, B_m, resulting from the persistent magnetization currents circulating in the superconducting filaments, and 3) a component, B_e, resulting from the cable eddy currents. In the current range where the saturation effects can be neglected, B_t varies linearly as a function of I. The B_m component is dominated by the critical current density of the superconductor and decreases with increasing I. The B_e component, however, only arises when the current is changed, and is expected to vary linearly as a function of $\partial I/\partial t$. In first approximation, a current ramp at a constant rate should thus result in a constant B_e.

The harmonics data presented in the previous section were rescaled using Eq. (2). The factors B_0 $(b_{nu} + b_{nd})/2$ and B_0 $(a_{nu} + a_{nd})/2$ can be interpreted as the contribution from the transport current. The functions plotted in figures 1 and 2 thus correspond to the contributions from the persistent magnetization currents and/or the eddy currents. In figure 2, the widths of the A_1 hystereses exhibited by magnets DCA314 and DCA315 appear to be constant as a function of current. This behavior is consistent what can be expected from a large eddy-

current contribution. On the other hand, in figure 1.a, the widths of the B_2 hysteresis appear to decrease as a function of current. This behavior is consistent with what can be expected from a large persistent-magnetization-current contribution. In the case of B_2, it also appears that the hysteresis width varies magnet-to-magnet, but that the differences in width are roughly constant as a function of current. These differences can be interpreted as resulting from eddy currents.

Let us now go back to our model, and let us first assume that the crossover resistance, r_c, is uniform throughout the coil. The AC-loss can be computed by integrating the power dissipated by the eddy currents in the crossover resistances. For a given current cycle, the model predicts that the AC-loss increases linearly as a function of ramp rate, with a slope inversely proportional to r_c. Considering the monopolar current cycle described in the previous section, it is then possible, for each magnet, to determine the value of r_c for which the slope of the calculated AC-loss versus ramp rate matches the slope of the experimental data. The results of these estimations are listed in Table 1. The value of r_c varies between 3 μΩ and 12 μΩ, depending on the magnet.

A uniform distribution of crossover resistances results in an eddy-current distribution that follows the dipole symmetries, and only effects the allowed multipoles. To explain an eddy-current contribution to the un-allowed multipoles, like that observed in figure 2, we have to assume that the crossover resistance is not uniform, but varies, from turn to turn, as a function of the azimuth. A first guess at a suitable azimuthal distribution of crossover resistances is obtained by considering that the main contribution to the eddy-current field comes from the eddy currents flowing near the coil inner radius. Replacing the coil by a cylindrical and non-uniform current sheet, it is then possible to determine the azimuthal current variations needed to generate the observed eddy-current field harmonics. The peaks and valleys of this current distribution indicates where the minima and extrema of the crossover resistance are located. Starting from this first guess, we can iterate on the full model, and determine a distribution of crossover resistances, that results in an eddy-current distribution, explaining both the observed field behavior and the measured AC-losses.

As an illustration, figures 3.a and 3.b show the distributions of crossover resistances and eddy currents obtained for the inner coils of magnet DCA314. (The outer coil crossover resistance is assumed to be uniform, equal to 20 μΩ). The coil quadrants, labelled Q-1 through Q-4, are defined by facing the magnet from the *non-lead end*. (The non-lead end is the magnet end opposite that where the current leads are located.). They are counted counterclockwise, starting from the top right quadrant. Figure 3.a shows the inner coil crossover resistance as a function of turn number. (The *pole turn* is the turn the closest to the collar pole, the *midplane turn* is the turn the closest to the coil midplane.) Figure 3.b shows the eddy currents flowing in the innermost and outermost strands of each turn of the inner coil for a ramp rate of 4 A/s. There appears to be, in each inner coil quadrant, a region of low crossover resistance, corresponding to an eddy current peak.

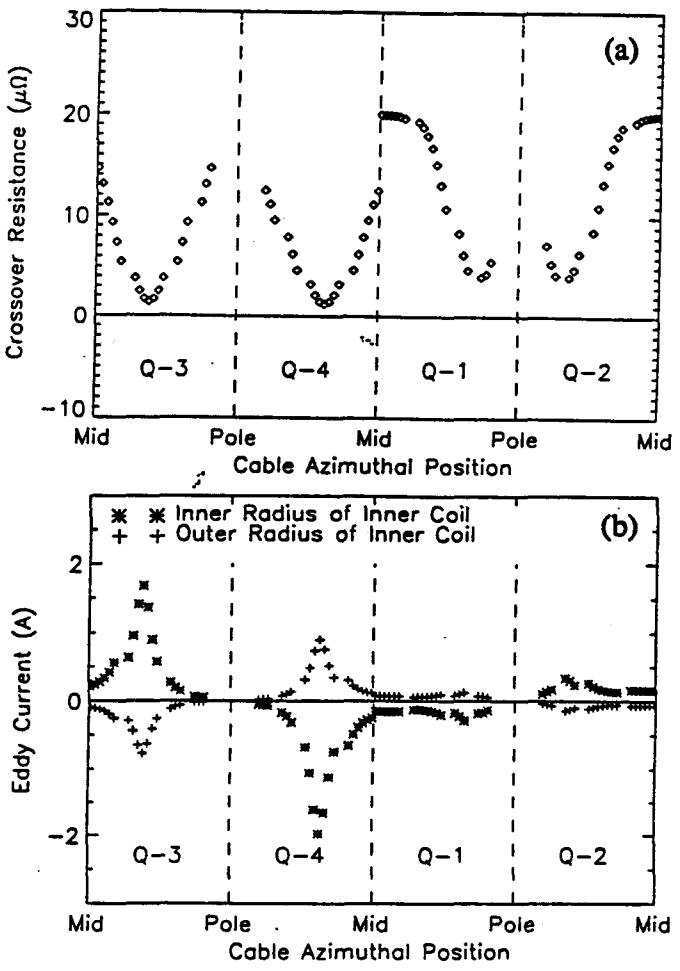

Fig. 3. Distribution of crossover resistances and eddy currents simulating the observed field behavior and measured AC-losses of magnet DCA314: a) crossover resistance distribution, and b) eddy current distribution.

Figure 4.a and 4.b show a comparison between the measured and computed A_1 and B_2. The stars correspond to the persistent magnetization current contribution computed by the DESY software, the crosses correspond to the eddy current contributions computed using the crossover resistance distribution described above, and the triangles correspond to their sum. (The eddy current contribution was calculated for a ramp rate of 4 A/s). The calculated harmonics agree well with the measurements for currents up to 4 kA, where saturation effects become important.

For the three magnets on which AC-loss measurements were performed, we were able to determine a distribution of crossover resistances that could explain both the AC-losses and the field behavior. In all three cases, there appears to be, in each quadrant of the inner coils, a region of low crossover resistance. The origin of these low crossover resistance regions has yet to be determined.

The model shows that, during an up-ramp, the eddy currents flowing near the coil inner radius have the same direction as the transport current, and, that, for ramp rates of the order of 100 A/s, they may be as large as 60 A for the innermost

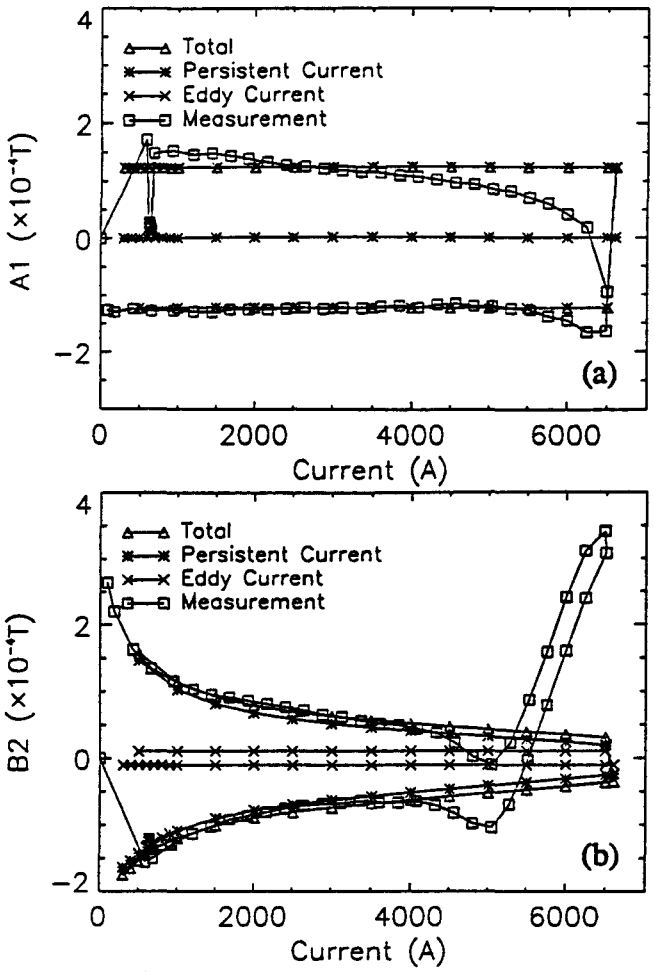

Fig. 4. Comparison between calculation and measurement of the field harmonics of magnet DCA314: a) A_1 vs. current and b) B_2 versus current.

strands. It results that the local margin, at the inner edge of the cable, where the magnetic field is the largest, can be significantly reduced. On the other hand, during a down-ramp, the direction of the eddy currents flowing at the coil inner radius is opposite to that of the transport current. This may eventually explain why, despite the dramatic degradation of the quench current observed at large up-ramp rate, the magnets did not quench on a down-ramp. In any case, the region of lowest crossover resistance, which corresponds to the region with the largest eddy currents and the largest AC losses, should correspond to the region where the large ramp-rate quenches originate. For magnets DCA312 and DCA315, the model predicts that the large ramp-rate quenches should originate in the upper inner coils, while, for magnet DCA314, they should originate in the lower inner coil. These predictions agree very well with the actual quench start localizations observed on these magnets at large ramp rates.

CONCLUSION

The cable eddy current model we have developed can successfully simulate the anomalous field behavior observed in some of the SSC 5-cm-aperture, 15-m-long dipole magnet prototypes. It is also consistent with the measured AC-losses and the localizations of the high ramp-rate quenches. The consistent agreements between simulations and experimental data give us good confidence that we have identified the cause of the poor AC-performance of these magnets. The next step is now to determine how to improve the cable properties.

ACKNOWLEDGEMENTS

The authors are grateful to R. Schermer, J. Tompkins, and P. Wanderer for many fruitful discussions. They also would like to thank C. Finck for her comments on the manuscript.

REFERENCES

[1] C.P. Bean, "Magnetization of Hard Superconductors," Phys. Rev. Lett., 8(6), 1962, pp. 250-253.

[2] P. Schmüser, "Superconducting Magnets for Particle Accelerators," AIP Conference Proceedings, 249(2), 1992, pp. 1099-1158.

[3] H. Brück, D. Gall, *et al.*, "Persistent Current Effects in the Superconducting HERA Magnets and Correction Coils," Proc. 2nd Eur. Part. Acc. Conf., 1990, pp 1160-1162.

[4] Y. Zhao, private communication.

[5] P. Wanderer, M. Anerella, *et al*, "A Summary of SSC Dipole Magnet Field Measurement", to appear in the proceedings of the 4th Annual International Industrial Symposium on the Super Collider, New Orleans, LA, USA, March 4-6, 1992.

[6] A. Devred, T. Bush, *et al.*, "Review of SSC Dipole Magnet Mechanics and Quench Performance," *ibid.*

[7] J. Strait, D. Orris, *et al.*, "Quench Performance of Fermilab/General Dynamics Built Full Length SSC Collider Dipole Magnets," *ibid.*

[8] G. Ganetis, J. Herrera, *et al.*, "Field Measuring Probe for SSC Magnets, Proc. 1987 IEEE Part. Acc. Conf., 1987, pp. 1393-1395.

[9] R.C. Gupta, J.G. Cottingham, *et al.*, "A Comparison of Calculations and Measurements of the Field Harmonics as a Function of Current in the SSC Dipole Magnets," Proc. 1991 IEEE Part. Acc. Conf., 1991, pp. 42-44.

[10] D. Christopherson, D. Capone, *et al.*, "SSC 40mm Cable Results and 50mm Design Discussions," IEEE Trans. Magn., 27(2), 1991, pp. 1881-1883.

[11] G.H. Morgan, "Eddy Currents in Flat Metal Filled Superconducting Braids," J. Appl. Phys., 44, 1973, pp. 3319-3322.

[12] T. Ogitsu, to be published.